Contents lists available at ScienceDirect

Nano Energy

journal homepage: www.elsevier.com/locate/nanoen

Communication

Boosting thin-film perovskite solar cell efficiency through vacuum-deposited sub-nanometer small-molecule electron interfacial layers

Wei-Hung Lee[a], Chien-Yu Chen[a], Chia-Shuo Li[b], Sheng-Yi Hsiao[a], Wei-Lun Tsai[a], Min-Jie Huang[c], Chien-Hong Cheng[c], Chih-I Wu[b,*], Hao-Wu Lin[a,*]

[a] Department of Materials Science and Engineering, National Tsing Hua University, No. 101, Section 2, Kuang-Fu Road, Hsinchu 30013, Taiwan
[b] Department of Electrical Engineering, N ational Taiwan University, No. 1, Sec. 4, Roosevelt Road, Taipei 10090, Taiwan
[c] Department of Chemistry, National Tsing Hua University, No. 101, Section 2, Kuang-Fu Road, Hsinchu 30013, Taiwan

ARTICLE INFO

Keywords:
Perovskite solar cells
Vacuum deposition
Electron interfacial layer
Pyridine derivatives

ABSTRACT

In this paper, we demonstrate that the performance of perovskite solar cells can be largely boosted with sub-nm pyridine-containing small-molecule electron interfacial layers. These vacuum-deposited sub-nm layers between perovskites and electron transport layers create a permanent dipole moment that improves the interfacial energy level alignment and facilitates a fast electron sweep-out. With these interfacial layers, the devices exhibit exceptional power conversion efficiencies up to 18.8%, a 25% increase compared to that of the one without the interfacial layer.

1. Introduction

Recently, halide perovskite semiconductors have attracted a great amount of attention because of their unique optoelectronic properties and potential applications in solar and dim-light energy conversion, light emission, lasing, transistors, and sensors [1–11]. Compared to current mainstream group IV and III–V semiconductors, halide perovskite thin films can be fabricated at much lower temperatures, which makes them suitable for low-cost and large-area production. Similar to aromatic organic semiconductors, semiconducting perovskite thin films can be fabricated by either solvent-based solution processes or solvent-free vacuum deposition. Owing to the different characteristics of deposition methods, two distinct approaches have been applied to solution-processed and vacuum-deposited perovskites to achieve high device performance. In the solution process, a complex perovskite composition can easily be realized by the mixture of perovskite precursor solutions, while in the vacuum process, without the issue of dissolution, effortless deposition of multiple layers is usually achieved [12]. In vacuum-deposition organic light-emitting diodes, sub-nanometer to few-nanometer interfacial layers, such as inorganic materials, MoO_x, CsF, and conjugated compounds, 1,4,5,8,9,11-hexaazatriphenylene hexacarbonitrile (HAT-CN) and 8-hydroxyquinolinato lithium (Liq), have been widely used for the effective injection of holes or electrons [13–16]. In this paper, we demonstrate that by taking the advantages of precise thickness control and solution-free layer-by-layer stacking, of the vacuum deposition, performance of perovskite solar cells can be largely boosted with sub-nm small-molecule electron interfacial layers (EILs). These vacuum-deposited sub-nm layers between perovskites and electron transport layers (ETLs) create a permanent dipole moment that improves the interfacial energy level alignment and facilitates a fast electron sweep-out. All perovskite solar cell performance parameters, including short-circuit current density (J_{SC}), open-circuit voltage (V_{OC}), and fill factor (FF), can be simultaneously enhanced, resulting in a 24.5% increase in power conversion efficiency (PCE).

2. Experimental section

2.1. Device fabrication

The devices were prepared on cleaned indium tin oxide (ITO) substrates. The substrates were then loaded into a high vacuum chamber (base pressure $< 1 \times 10^{-6}$ Torr) to deposit MoO_3 and tris[4-(5-phenylthiophen-2-yl)phenyl]amine) (TPTPA) thin films layer by layer, and the perovskite films were then fabricated by sequential vacuum deposition, which is reported in another paper [2]. After the formation of perovskite, we deposited 1,3,5-Tri[(3-pyridyl)-phen-3-yl] benzene (TmPyPB), 4,6-Bis(3,5-di(pyridin-4-yl)phenyl)-2-methylpyrimidine (B4PyMPM), and Tris(2,4,6-trimethyl-3-(pyridin-3-yl)phenyl) borane (3TPYMB) as EILs respectively. During the interfacial layer deposition, the deposition rate was maintained at 0.1 Å s^{-1}. After that, C_{60}, TmPyPB, and Ag were deposited layer by layer. The thicknesses of

* Corresponding authors.
E-mail addresses: chihiwu@ntu.edu.tw (C.-I. Wu), hwlin@mx.nthu.edu.tw (H.-W. Lin).

http://dx.doi.org/10.1016/j.nanoen.2017.05.049
Received 28 April 2017; Received in revised form 22 May 2017; Accepted 23 May 2017
Available online 24 May 2017

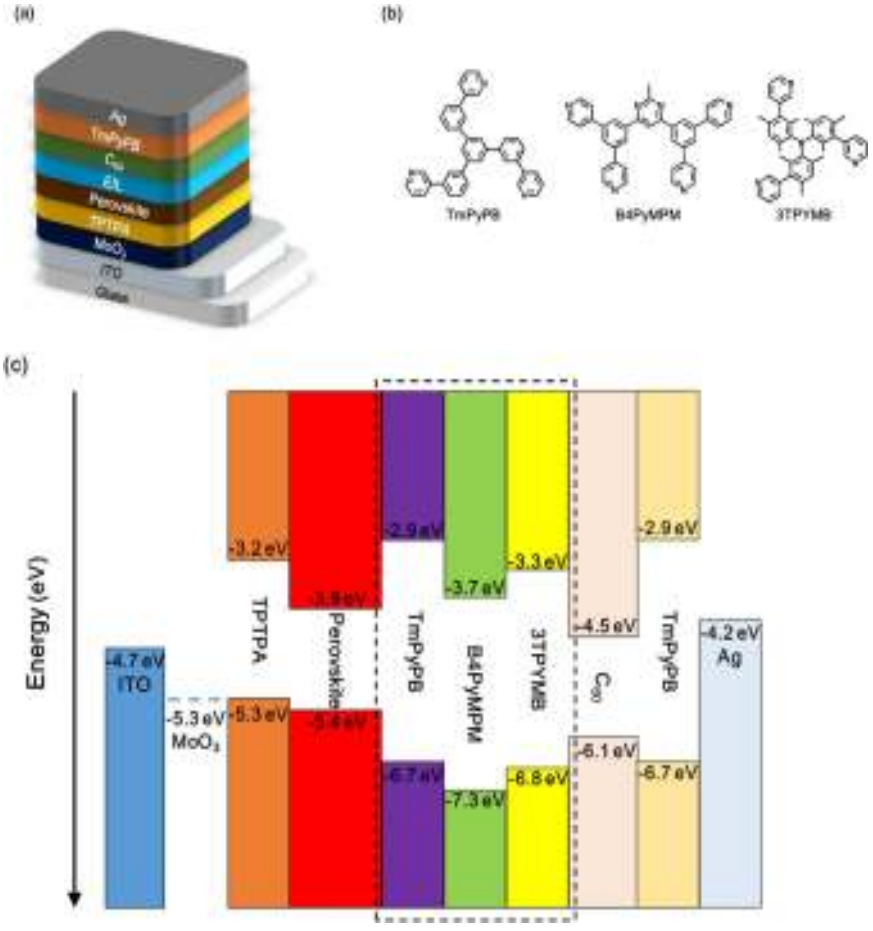

Fig. 1. (a) The device structure of perovskite solar cells. (b) Chemical structures of materials utilized as EILs. (c) Energy diagram of the devices utilized in this study.

the organic layers were all carefully calibrated by using spectroscopic ellipsometry. The devices were configured as glass substrate/ITO (145 nm)/MoO_3 (5 nm)/TPTPA (10 nm)/$CH_3NH_3PbI_3$ (370 nm) /EIL (0.5 nm)/C_{60} (90 nm)/TmPyPB (7 nm)/Ag (150 nm). The device areas (0.051 cm^2) were defined by shadow masks. The devices were encapsulated using UV-cured sealant (Everwide Chemical Co.) and cover glasses after fabrication, and were subsequently characterized in air.

2.2. Device measurement and characterization

The *J*–V characteristics of the devices were measured using a Keithley 2636B SourceMeter in the dark and under AM1.5 G simulated solar illumination with an intensity of 100 mW cm^{-2} (1 sun, calibrated by an NREL-traceable KG5-filtered silicon reference cell). Normally, the scan direction travels from the positive to negative bias with a step size of 10 mV and a delay time between points of 300 ms. The external quantum efficiency (EQE) spectra were acquired by illuminating the solar cells with chopped monochromatic light with continuous-wave-biased white light (from a halogen lamp). The photocurrent signals were extracted with the lock-in technique using a Stanford Research System current preamplifier followed by an Ametek lock-in amplifier. The intensity of the monochromatic light was calibrated with a NIST-traceable Ophir power meter. Transient photocurrent and transient photovoltage measurements were performed using the second harmonic of a Nd:YAG laser (532 nm) as an excitation source. A 100 W variable-intensity halogen lamp was used as the bias light. The transient photocurrent signals were amplified using a variable-gain high-speed current amplifier (FEMTO, DHPCA-100), and the transient signals were recorded using a Tektronix oscilloscope (DPO3050). Averages of 256 traces were calculated to improve the signal-to-noise ratio. The average lifetimes were fitted with bi-exponential decay functions.

2.3. AFM, UPS and XPS measurements

Atomic force microscopy (AFM) images were measured with a Bruker Dimension Icon® Atomic Force Microscope operating in a tapping mode. Photoemission measurements were conducted in two connected ultrahigh vacuum chambers, one for organic thermal deposition and the other for spectroscopic analysis with a base pressure of 1×10^{-9} Torr. To avoid the difference induced by processing conditions, the perovskite films were prepared simultaneously and were then stored in a nitrogen atmosphere. The prepared perovskite film was loaded into the analysis chamber as quick as possible after exposure to the air to prevent contamination. C_{60} and 3TPYMB were thermally deposited on the perovskite film under a pressure of 5×10^{-7} Torr with a deposition rate of 0.2 Å/s using a Sycon STM-100 crystal thickness monitor, and the XPS and UPS spectra were acquired immediately after every deposition. The valance-band UV photoemission spectra were obtained using HeI (21.2 eV) as the excitation source and photoemitted electrons were counted by a hemispherical analyzer with an overall resolution of 0.05 eV. The absolute energy scale of the UPS and XPS spectra is relative to the Fermi edge and the 4f core level of a sputter-cleaned gold substrate, respectively. To eliminate the analyzer effect, a sample bias of −5 eV was applied when acquiring the secondary electron cutoff spectra.

2.4. Molecular computational details

Geometric optimizations were carried out with density functional theory implemented in the Gaussian 09 package. Becke's three-parameter functional combined with Lee, Yang, and Parr's hybrid exchange correlation functional (B3LYP) with the 6–31G* basic set was utilized for all atoms. Harmonic vibrational frequencies were performed on the optimized geometries to confirm energetic minima. The molecular

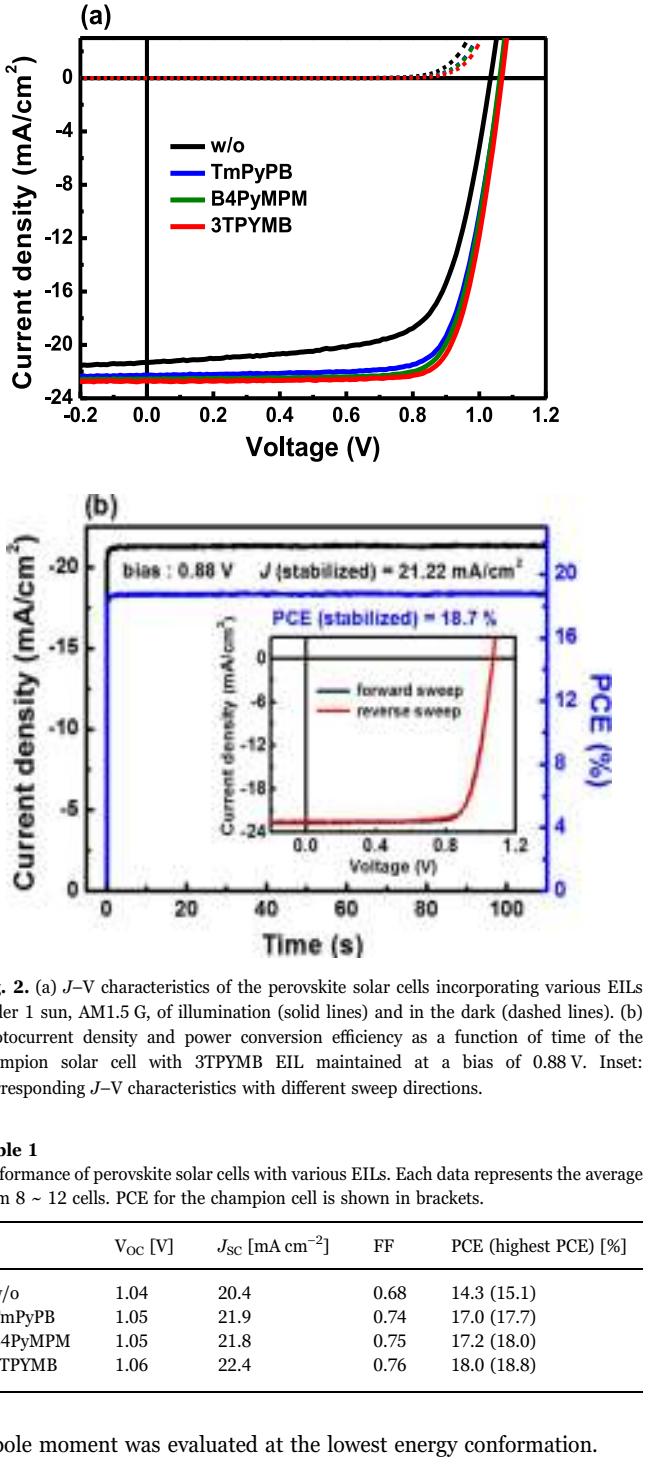

Fig. 2. (a) *J*–V characteristics of the perovskite solar cells incorporating various EILs under 1 sun, AM1.5 G, of illumination (solid lines) and in the dark (dashed lines). (b) Photocurrent density and power conversion efficiency as a function of time of the champion solar cell with 3TPYMB EIL maintained at a bias of 0.88 V. Inset: Corresponding *J*–V characteristics with different sweep directions.

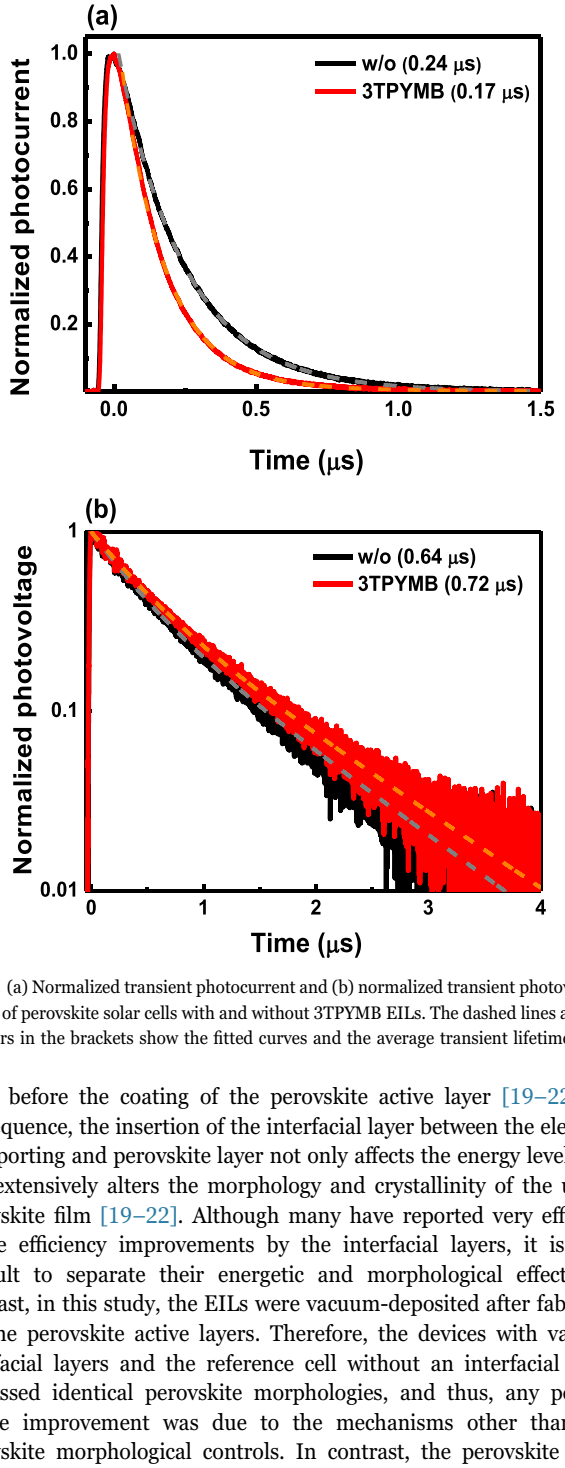

Fig. 3. (a) Normalized transient photocurrent and (b) normalized transient photovoltage results of perovskite solar cells with and without 3TPYMB EILs. The dashed lines and the numbers in the brackets show the fitted curves and the average transient lifetimes.

Table 1
Performance of perovskite solar cells with various EILs. Each data represents the average from 8 ~ 12 cells. PCE for the champion cell is shown in brackets.

	V_{OC} [V]	J_{SC} [mA cm^{-2}]	FF	PCE (highest PCE) [%]
w/o	1.04	20.4	0.68	14.3 (15.1)
TmPyPB	1.05	21.9	0.74	17.0 (17.7)
B4PyMPM	1.05	21.8	0.75	17.2 (18.0)
3TPYMB	1.06	22.4	0.76	18.0 (18.8)

dipole moment was evaluated at the lowest energy conformation.

3. Results and discussion

Fig. 1a displays the device structure of the solar cells used in this study. Vacuum-sublimable small-molecule electron transporting materials, TmPyPB, B4PyMPM, and 3TPYMB were inserted between the vacuum-deposited $CH_3NH_3PbI_3$ perovskite active layer and C_{60} ETL. The molecular structures of the electron interfacial materials are displayed in Fig. 1b. Fig. 1c displays the energy band diagram. The interfacial materials used all possess high-energy bandgaps with low-lying HOMO and high-lying LUMO levels. The low-lying HOMO levels may block the photogenerated holes from diffusing to the C_{60} ETLs. However, the high-lying LUMO levels also inhibit the electrons from transporting to the C_{60} ETLs; hence, it is possible that the tunneling mechanism is operational in the efficient devices [17,18].

In previous EIL studies, the interfacial layers were usually fabricated before the coating of the perovskite active layer [19–22]. In consequence, the insertion of the interfacial layer between the electron transporting and perovskite layer not only affects the energy levels but also extensively alters the morphology and crystallinity of the upper perovskite film [19–22]. Although many have reported very efficient device efficiency improvements by the interfacial layers, it is very difficult to separate their energetic and morphological effects. In contrast, in this study, the EILs were vacuum-deposited after fabricating the perovskite active layers. Therefore, the devices with various interfacial layers and the reference cell without an interfacial layer possessed identical perovskite morphologies, and thus, any performance improvement was due to the mechanisms other than the perovskite morphological controls. In contrast, the perovskite films with ultrathin sub-nm EILs in this study exhibited identical morphology as indicated in Fig. S1, implying the effects of the EILs are purely energetic.

Fig. 2a displays the solar cell *J*–V characteristics of the devices without and with 0.5-nm EILs under a simulated illumination of 1 sun. The performance parameters are summarized in Table 1 and their EQE spectra are presented in Fig. S2 in the supporting information. Intriguingly, 3TPYMB, B4PyMPM, and TmPyPB devices exhibit clear improvements compared with the best reference cell without EIL. The common characteristic of 3TPYMB, B4PyMPM, and TmPyPB are that they all consist of pyridine chromophores. Notably, the device with the 3TPYMB interfacial layer exhibited a high J_{SC} of 22.7 mA/cm^2, V_{OC} of 1.07 V, FF of 0.77, and PCE of 18.8%, which corresponds to 6.6%, 2.9%, 13.5%, and 24.5% enhancements in J_{SC}, V_{OC}, FF, and PCE, respectively. The device also exhibited a high stabilized PCE of 18.7% and no *J*–V sweeping hysteresis, as shown in Fig. 2b. The B4PyMPM

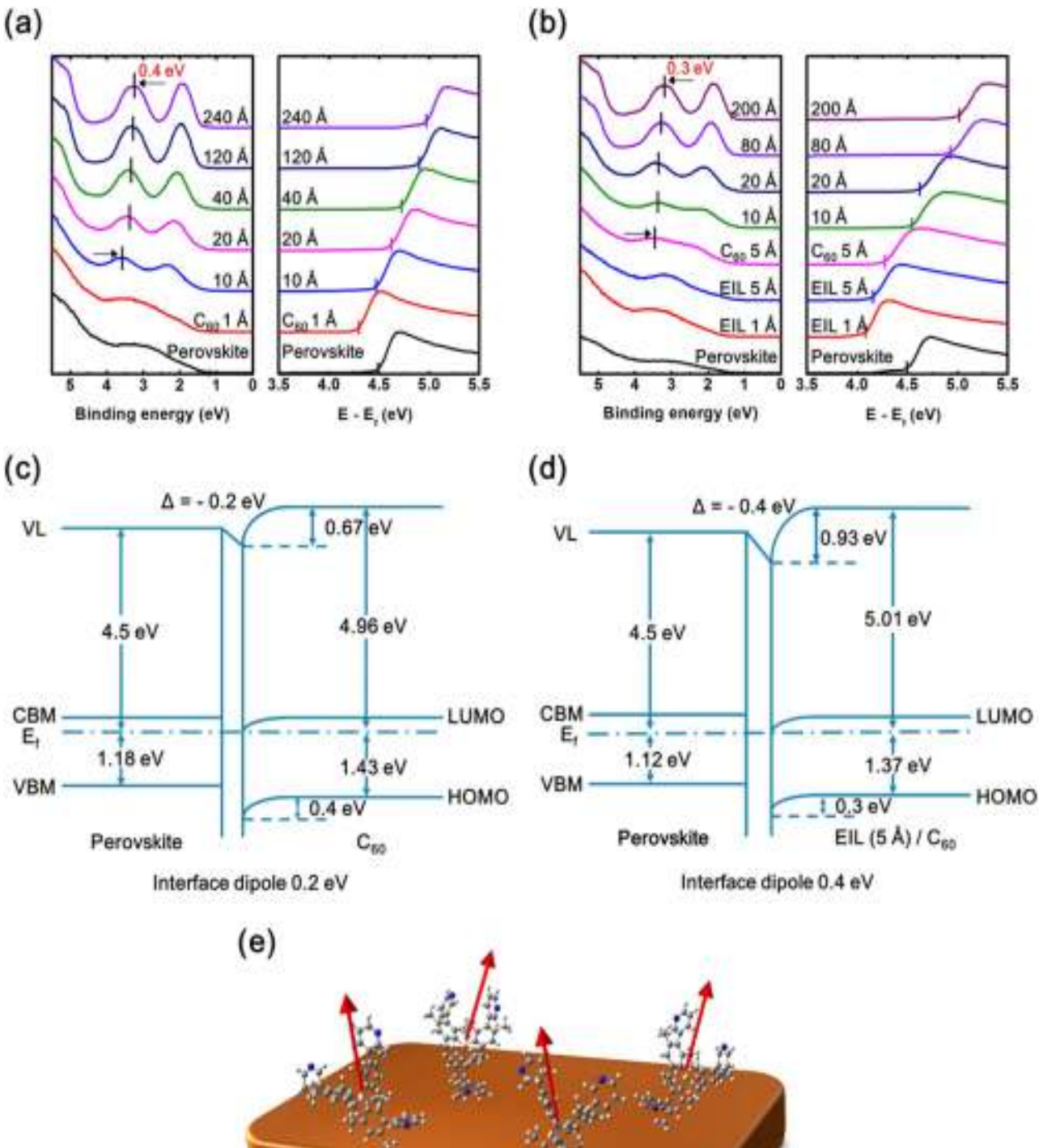

Fig. 4. UPS spectral evolution of various (a) C_{60} and (b) 3TPYMB/C_{60} thicknesses on the perovskite film. (c) Interfacial electronic structure of perovskite/C_{60} and (d) perovskite/3TPYMB/C_{60}. (e) Illustration of the 0.5-nm vacuum-deposited 3TPYMB molecules on the perovskite film. The arrows represent permanent dipole moments with respect to the molecules.

and TmPyPB also exhibited negligible hysteresis, as indicated in Fig. S3 in the supporting information. The *J*–V characteristics of the TmPyPB, B4PyMPM and 3TPYMB devices of different delay times in between the voltage points are shown in Fig. S4–S6. Negligible hysteresis was found at all sweeping speeds. The approximately 19% PCE in both the *J*–V sweeping and stabilized PCEs of the 3TPYMB cells are among the highest values reported in vacuum-deposited perovskite solar cells and are a step closer to state-of-the-art solution-processed devices (PCE 22.1%) [23].

To further investigate the origins of the performance improvement of the 3TPYMB champion cell, transient photocurrent and transient photovoltage measurements were performed. As shown in Fig. 3a, the device with the 3TPYMB interfacial layer exhibited a faster transient photocurrent decay (with a decay lifetime of 0.17 μs) than the device without the interfacial layer (decay lifetime = 0.24 μs), revealing that the carrier extraction efficiency was enhanced by the incorporation of

the 3TPYMB interfacial layer. Fig. 3b displays the transient photovoltage measurement results. The extracted average recombination lifetimes are 0.72 and 0.64 μs for the 3TPYMB device and the reference device without interfacial layer, respectively. The retarded recombination rate indicates a slower carrier recombination rate in the 3TPYMB device, which also explains the improvement in V_{OC} and FF of the 3TPYMB device in the *J*–V measurement. The photocurrent density (J_{ph}) *vs*. effective voltage (V_O-V, where V is the applied voltage and V_O is the voltage at which $J_{ph} = 0$) plot is shown in Fig. S7. The 3TPYMB device exhibited smaller slopes at both high effective voltage (0.2 V < V_O-V < 1.1 V) and lower effective voltage (0.04 V < V_O-V < 0.2 V) ranges compared with the reference cell. These results also suggest an improved carrier transport and the minimization of the recombination.

With the above-mentioned measurement results, the fast electron sweep-out and retarded recombination natures of the 3TPYMB device were confirmed. We suspected that these preferable characteristics were caused by the interfacial dipoles created by the vacuum-deposited sub-nm 3TPYMB layer. Hence, *in-situ* UV and X-ray photoemission spectroscopies (UPS and XPS) were utilized to investigate the energy-level evolution. 3TPYMB and C_{60} were incrementally deposited *in-situ* on the perovskite film and XPS and UPS spectra were acquired after each deposition. Fig. 4a and b show the evolution of the valence band (left panel) and vacuum level (VL) position (right panel) of the perovskite/C_{60} and perovskite/0.5 nm 3TPYMB/C_{60} thin films, respectively. The valence band maximum (VBM) (or HOMO) and work function (WF) were extracted by linearly extrapolating the leading edge of the VB and the onset of the secondary cutoff to the background, respectively. The conduction band maximum and LUMO were determined by considering the optical band gaps of the materials. The VBM (or HOMO) and WF were about 1.1 and 4.5 eV for the pristine perovskite film and approximately 1.4 and 5.0 eV for the bare C_{60}, respectively, in the perovskite. These values are consistent with the published values in the literature for the $CH_3NH_3PbI_3$ perovskite and C_{60} thin films [24]. Fig. 4c and d illustrate the interfacial electronic structures of the perovskite/C_{60} and perovskite/0.5 nm 3TPYMB/C_{60} thin films extracted from the UPS and XPS (shown in Fig. S8) measurements. In the perovskite/C_{60} sample, the very first C_{60} deposition leads to a 0.2 eV downward shift in VL, which is in accordance with the previous report and is attributed to the charge-transfer-induced interfacial dipole formation at the perovskite/C_{60} interface [25]. Notably, by the introduction of a 0.5 nm 3TPYMB, an even higher 0.4 eV downward shift in VL is observed. In addition, a smaller 0.3 eV shift in the C_{60} HOMO peak is noted in the perovskite/0.5 nm 3TPYMB/C_{60} sample compared with the value of 0.4 eV in the perovskite/C_{60} sample. The results can be ascribed to a smaller band bending in C_{60} in the perovskite/0.5 nm 3TPYMB/C_{60} sample. By incorporating a 0.5-nm 3TPYMB between the perovskite and C_{60}, a much stronger interfacial dipole was formed at the perovskite/C_{60} interface and less band bending was observed in the C_{60} region. Both facilitate effortless electron transportation from the perovskite layer towards the cathode.

The strong interfacial dipoles formed by sub-nm EILs were believed to be related to a preferable molecular orientation upon vacuum deposition. The direction of permanent dipole moments with respect to the 3TPYMB, B4PyMPM, and TmPyPB molecules were calculated and are displayed in Fig. S9 in the supporting information. With the interfacial energy band structures and computed molecular dipole moments, we plotted the illustration of the 0.5-nm vacuum-deposited 3TPYMB molecules on the perovskite underlayer, as shown in Fig. 4e. The 3TPYMB molecules substantially exhibited a preferable orientation with the permanent dipole moments pointed outwards, resulting in a stronger interfacial dipole of 0.4 eV pointed outwards towards the cathode direction. When further increasing the 3TPYMB, B4PyMPM, and TmPyPB layer thicknesses, the device performance gradually decreased, and the results are presented in Fig. S10. These results indicate that the preferable orientation of the vacuum deposited interfacial layers only occurs in the first few angstroms of the films, presumably due to the interaction of the perovskite surface and the deposited molecules.

4. Conclusions

In summary, we demonstrated that by the insertion of vacuum-deposited sub-nm pyridine-containing EILs, the performance of perovskite solar cells can largely be increased to approximately 19% PCE, a 25% increase compared to that of the one without the interfacial layer. The UPS and XPS results indicated that the effect of these interfacial layers was the creation of a strong interfacial dipole, which was beneficial to the photoelectron extraction towards external circuitry. The retarded carrier recombination and fast carrier sweep-out were also confirmed by transient photovoltage and transient photocurrent measurements. Owing to the layer-by-layer deposition and underlayer-insensitive natures of vacuum sublimation, we envision that these vacuum-deposited sub-nm EILs can be universally applied to various kinds of vacuum-deposited as well as solution-processed perovskite active layers of a variety of compositions.

Acknowledgment

The authors would like to acknowledge the financial support from the Ministry of Science and Technology of Taiwan (MOST 105–2112-M-007–016-MY3, MOST 105–2628-E-007–008-MY3, MOST 105–2633-M-007-003), and National Tsing Hua University.

Appendix A. Supporting information

Supplementary data associated with this article can be found in the online version at doi:10.1016/j.nanoen.2017.05.049.

References

[1] C.-W. Chen, H.-W. Kang, S.-Y. Hsiao, P.-F. Yang, K.-M. Chiang, H.-W. Lin, Adv. Mater. 26 (2014) 6647–6652.
[2] S.-Y. Hsiao, H.-L. Lin, W.-H. Lee, W.-L. Tsai, K.-M. Chiang, W.-Y. Liao, C.-Z. Ren-Wu, C.-Y. Chen, H.-W. Lin, Adv. Mater. 28 (2016) 7013–7019.
[3] C.-Y. Chen, H.-Y. Lin, K.-M. Chiang, W.-L. Tsai, Y.-C. Huang, C.-S. Tsao, H.-W. Lin, Adv. Mater. 29 (2017) 1605290.
[4] J. Gong, S.B. Darling, F. You, Energy Environ. Sci. 8 (2015) 1953–1968.
[5] N.-G. Park, Mater. Today 18 (2015) 65–72.
[6] C.-Y. Chen, J.-H. Chang, K.-M. Chiang, H.-L. Lin, S.-Y. Hsiao, H.-W. Lin, Adv. Funct. Mater. 25 (2015) 7064–7070.
[7] Y.-H. Kim, H. Cho, J.H. Heo, T.-S. Kim, N. Myoung, C.-L. Lee, S.H. Im, T.-W. Lee, Adv. Mater. 27 (2015) 1248–1254.
[8] H. Cho, S.-H. Jeong, M.-H. Park, Y.-H. Kim, C. Wolf, C.-L. Lee, J.H. Heo, A. Sadhanala, N. Myoung, S. Yoo, S.H. Im, R.H. Friend, T.-W. Lee, Science 350 (2015) 1222–1225.
[9] T. Matsushima, S. Hwang, A.S.D. Sandanayaka, C. Qin, S. Terakawa, T. Fujihara, M. Yahiro, C. Adachi, Adv. Mater. 28 (2016) 10275–10281.
[10] G. Xing, N. Mathews, S.S. Lim, N. Yantara, X. Liu, D. Sabba, M. Grätzel, S. Mhaisalkar, T.C. Sum, Nat. Mater. 13 (2014) 476–481.
[11] D. Forgács, L. Gil-Escrig, D. Pérez-Del-Rey, C. Momblona, J. Werner, B. Niesen, C. Ballif, M. Sessolo, H.J. Bolink, Adv. Energy Mater. 7 (2016) 1602121.
[12] D. Bi, W. Tress, M.I. Dar, P. Gao, J. Luo, C. Renevier, K. Schenk, A. Abate, F. Giordano, J.-P. Correa Baena, J.-D. Decoppet, S.M. Zakeeruddin, M.K. Nazeeruddin, M. Grätzel, A. Hagfeldt, Sci. Adv. 2 (2016) e1501170.
[13] Y.-K. Kim, J.W. Kim, Y. Park, Appl. Phys. Lett. 94 (2009) 063305.
[14] H.-W. Lin, W.-C. Lin, J.-H. Chang, C.-I. Wu, Org. Electron. 14 (2013) 1204–1210.
[15] J.-A. Yoon, Y.-H. Kim, N.H. Kim, S.I. Yoo, S.Y. Lee, F.R. Zhu, W.Y. Kim, Nanoscale Res. Lett. 9 (2014) 191–197.
[16] Y. Lee, J. Kim, S. Kwon, C.-K. Min, Y. Yi, J.W. Kim, B. Koo, M. Hong, Org. Electron. 9 (2008) 407–412.
[17] J. Wei, H. Li, Y. Zhao, W. Zhou, R. Fu, H. Pan, Q. Zhao, Chem. Commun. 52 (2016) 10791–10794.
[18] Q. Wang, Q. Dong, T. Li, A. Gruverman, J. Huang, Adv. Mater. 28 (2016) 6734–6739.
[19] Y. Bai, H. Chen, S. Xiao, Q. Xue, T. Zhang, Z. Zhu, Q. Li, C. Hu, Y. Yang, Z. Hu, F. Huang, K.S. Wong, H.-L. Yip, S. Yang, Adv. Funct. Mater. 26 (2016) 2950–2958.
[20] S.M. Jain, Z. Qiu, L. Haggman, M. Mirmohades, M.B. Johansson, T. Edvinsson, G. Boschloo, Energy Environ. Sci. 9 (2016) 3770–3782.
[21] J. Zhang, P. Wang, X. Huang, J. Xu, L. Wang, G. Yue, X. Lu, J. Liu, Z. Hu, Q. Wang, Y. Zhu, RSC Adv. 6 (2016) 9090–9095.

[22] Q. Wu, W. Zhou, Q. Liu, P. Zhou, T. Chen, Y. Lu, Q. Qiao, S. Yang, ACS Appl. Mater. Inter. 8 (2016) 34464–34473.
[23] K. Mahmood, B.S. Swain, A. Amassian, Adv. Energy Mater. 5 (2015) 1500568–1500578.
[24] P. Schulz, L.L. Whittaker-Brooks, B.A. MacLeod, D.C. Olson, Y.-L. Loo, A. Kahn, Adv. Mater. Inter. 2 (2015) 1400532–1400536.
[25] P. Amsalem, J. Niederhausen, A. Wilke, G. Heimel, R. Schlesinger, S. Winkler, A. Vollmer, J.P. Rabe, N. Koch, Phys. Rev. B 87 (2013) 035440–035452.

Wei-Hung Lee is currently a graduate student at Department of Materials Science and Engineering, National Tsing-Hua University. His research interests include the transporting layers for perovksite solar cells and vacuum deposition technique for perovskite thin-film fabrication.

Chien-Yu Chen received his bachelor degree from National Tsing Hua University in 2014. He is presently a Ph. D. student at department of materials science and engineering at National Tsing Hua University. His research mainly focuses on perovskite solar cells and their applications.

Chia-shuo Li is a PhD student at Professor Chih-I Wu's group in the Graduate Institute of Electro-Optical Engineering of National Taiwan University. His research interests include perovskite solar cells and photoemission spectroscopy.

Sheng-Yi Hsiao graduated with a MS degree in the Department of Chemical Engineering at National Chung Hsing University. In 2013, Sheng-Yi joined the Advanced Optoelectronic Materials Research Group, National Tsing Hua University, to pursue his PhD under the supervision of Prof. Hao-Wu Lin. His current research interests are organic photovoltaics and perovskite solar cell.

Wei-Lun Tsai is a PhD student who majors in Materials Science and Engineering at National Tsing-Hua University. He is now studying the perovskite solar cells in Advanced Optoelectronic Materials Research Group under the supervision of Prof. Hao-Wu Lin. The primary research is charge transporting materials utilized in perovskite solar cells.

Min-Jie Huang received his BS (2004) and MS (2006) degrees from National Tsing Hua University (NTHU). His PhD degree was awarded in 2013 from National Taiwan University under the advisement of Prof. Chun-hsien Chen. Currently, he works as a postdoctoral researcher in the group of Professor Chien-Hong Cheng. His research interests focus on the theoretical studies of novel organic materials for electronic and photonic applications.

Chien-Hong Cheng received his Ph.D. from University of Rochester with Prof. Richard Eisenberg. After postdoctoral work in the same laboratory, he joined the Department of Chemistry at National Tsing Hua University (NTHU). Professor Cheng served as the Director General of the Department of Natural Sciences, National Science Council; President of Chemical Society, Taiwan; and Vice President for Academic Affairs of NTHU. In 2009, he was elected as a Fellow of the Royal Society of Chemistry and is currently a Chair Professor of NTHU. His research interests include transition metal-catalyzed organic reactions and organic materials in optoelectronics.

Chih-I Wu is a Professor in the Graduate Institute of Electro-Optical Engineering and the Department of Electrical Engineering at National Taiwan University. He received his Ph.D. degree in the Department of Electrical Engineering at Princeton University (1999). His main research area focuses on optical-electronic devices and materials and semiconductor physics, which includes organic light emitting materials, metal-semiconductor interfaces, and heterojunctions in electronic devices and optical-electronics.

Hao-Wu Lin is a Professor of Department of Materials Science and Engineering at National Tsing-Hua University (NTHU) in Taiwan. He received his Ph.D. degree from graduate institute of photonics and optoelectronics, National Taiwan University in 2007. Before joining NTHU in 2009, he worked at AU Optronics Corp. for research and development on organic light emitting displays. His current research interests include organic semiconductors for optoelectronic and electronic devices, next-generation photovoltaics, display technologies and nanoscience.